Sol-gel synthesis and physical properties of CuO:La nanocomposite thin films

N. TOUKA[1,*], D. TABLI[1], M. M. BOUGHANEM[1], N. SELMI[2]
[1]*Laboratory of Physics of Materials and Optoelectronic Components, Department of Physics, University of Bouira, Algeria*
[2]*Nuclear Research Centre of Birine, Algeria*

CuO and CuO: La nanocomposite thin films have been deposited by the sol-gel process using the spin coating technique. Lanthanum at two different concentrations was introduced in thin layers having a thickness corresponding to three layers. The structural characterization by XRD reveals that the deposited CuO and La doped CuO thin films are monoclinic and cubic crystals structures successively, and also notes the presence of lanthanum copper oxide (La_2CuO_4) which proves the insertion of dopant in the matrix, and the crystallite size of the films pure was affected by La concentration and was found to be decreased with the increase of La concentration. Raman measurement of CuO pure and CuO: La nanocomposite thin films confirmed the structure of CuO and Cu_2O. SEM studies revealed a uniform and relatively dense surface with small pyramids enveloping the nanometric-sized crystallite. It was found that the value of the optical energy gap increases with increasing of La for all samples.

(Received June 7, 2024; accepted December 2, 2024)

Keywords: Sol-gel, Copper oxide, La, Thin films, Physical properties

1. Introduction

For a long time, significant efforts have been made to explore new types of environmentally friendly materials for various applications. Semiconducting materials play a leading role in achieving this valuable goal. In particular, semiconducting metal oxides are considered the most attractive due to their exceptional physical and chemical properties, making them suitable for a wide range of applications [1,2]. Among them, copper oxide (CuO) and cuprous oxide (Cu_2O) stand out as promising candidates due to their unique properties [3,4].

CuO, a p-type semiconductor, exhibits a narrow bandgap (1.2 eV) and a high absorption coefficient (~ 10^5 cm^{-1}) [5,6] making it suitable for applications in optoelectronics, LEDs, sensors, photovoltaics, magnetic storage devices, and lithium-ion batteries [7-10]. Its non-toxicity, biocompatibility, and availability further enhance its appeal for various technological applications [11-13]. On the other hand, Cu_2O, also a p-type semiconductor, has a bandgap of 2.17 eV and a cubic crystal structure [14,15]. It is particularly promising for photovoltaic applications due to its ability to convert solar energy into electricity efficiently [16].

The remarkable properties of copper oxides can be attributed to their unique electronic structures. In CuO, the narrow bandgap facilitates efficient light absorption, making it an excellent material for applications requiring high optical absorption. In Cu_2O, the presence of copper vacancies introduces acceptor levels, enhancing its p-type conductivity and making it suitable for applications in transparent electronics and solar cells.

To exploit these properties, copper oxide thin films can be synthesized using various methods. These methods include: Sol-Gel method. This is a versatile and cost-effective technique for preparing metal oxide films. It involves the hydrolysis and condensation of metal alkoxides or metal salts to form a sol, which is then deposited on a substrate and converted into a gel. The gel is subsequently dried and annealed to form a thin film. The sol-gel method allows precise control over the film's composition and thickness. Spin Coating: Often used in conjunction with the sol-gel method, spin coating involves depositing a small amount of the sol on a substrate, which is then spun at high speed to spread the sol uniformly. This technique is simple, scalable, and capable of producing uniform thin films with controlled thickness [17]. Among the other methods we mention: Chemical Vapor Deposition (CVD) [18], Physical Vapor Deposition (PVD) [19], Hydrothermal Synthesis [20] and Electrodeposition [21].

In this work, we present the fabrication and characterization of lanthanum-doped copper oxide thin films, prepared by the sol-gel method and deposited by spin coating. The characterization of the doped thin films was carried out using techniques such as X-ray diffraction (XRD), Raman spectroscopy, UV-Visible spectroscopy and scanning electron microscopy (SEM). The obtained results show notable modifications in the structure, bond vibrations, morphology, and optical properties of the doped thin films, highlighting their considerable value in scientific and industrial fields due to their novel characteristics.

2. Experimental

The precursor solutions for both undoped and La doped CuO were prepared by the sol-gel method using copper (II) chloride anhydrous ($CuCl_2$) (98%, Biochem) and lanthanum nitrate [$La(NO3)_3$ $3H_2O$] (98%, Sigma Aldrich) as the starting materials. The details of the preparation of the undoped solution have been described elsewhere [22] except that in this work the quantity of the solvent methanol (CH_3OH) is 15 ml. La doping solution was prepared by dissolving lanthanum nitrate [$La(NO_3)_3$ $3H_2O$] in undoped solution, to get a rate mass doping of 5% and 7% we dissolving 0.2 g and 0.3 g in 15 mL successively. The solution becomes homogeneous after stirring at 60 °C for 10 min.

Before deposition, the glass substrates were successively cleaned with acetone, ethanol, and deionized water in an ultrasonic bath. Undoped and La doped CuO thin films were deposited on the glass substrates by spin coating technique at room temperature, with a speed of 2800 rpm for 30 s. After each spin-coating process, the films were kept on a hot plate at 100 °C in air for 10 min to remove the organic contaminants. This cycle of the coating and drying process (one layer) was repeated to produce undoped and La doped CuO thin films with a thickness corresponding to three layers. Finally, all the films were annealed in air, at 350 °C for 2 h.

The structural properties of the films have been studied by X-ray diffraction (XRD) using a PANalytical X'Pert PRO Diffractometer by scanning through 2θ angle of 25-60° with $Cu_{K\alpha}$ irradiation (λ $Cu_{K\alpha}$ = 1.5418 Å). Raman spectra were recorded by using a spectrometer (LabRAM HR Horiba Jobin Yvon) equipped with a HeNe laser providing an excitation wavelength of 632 nm. The surface morphologies of the deposited films were characterized by field emission scanning electron microscopy (JSM-7610F Plus). The optical absorption spectra were recorded using an UV-Vis-NIR spectrophotometer (Shimadzu, UV-3101 PC) in the wavelength range 300-800 nm. All measurements were carried out at room temperature.

3. Results and discussion

3.1. Structural analysis

Fig. 1 shows the adjustment of the undoped thin films diffraction spectrum using the High Score plus software and compared with JCPDS cards N° (98-005-3322) and N° (00-045-0937) shows the presence of two phases tenorite (CuO) of structure monoclinic and cuprite (Cu_2O) of structure cubic in the pure thin layers with 84% cuprite and 16% tenorite. Fig. 2 shows the adjustment of the diffraction spectrum of thin layers of copper oxide doped with La 5%, using the High Score plus software shows the presence of two phases, tenorite (CuO) (monoclinic structure) with 71% and the cuprite phase (Cu_2O) (cubic structure) with 9%, and we observe a characteristic peak of lanthanum that of La_2CuO_4; which resulted from La^{3+} ions when cooperate with the CuO particle matrix to form La-Cu-O solid solutions since the radius of La^{3+} (r = 1.95 Å) is larger than that of Cu^{2+} (r =1.28 A°); the difference in the ionic radii of the host and the dopant atom results in changes in the lattice parameters of the system. Fig. 3 shows the adjustment of the diffraction spectrum of thin layers of copper oxide doped with 7%, we observe that the presence of only one phase of tenorite (monoclinic structure).

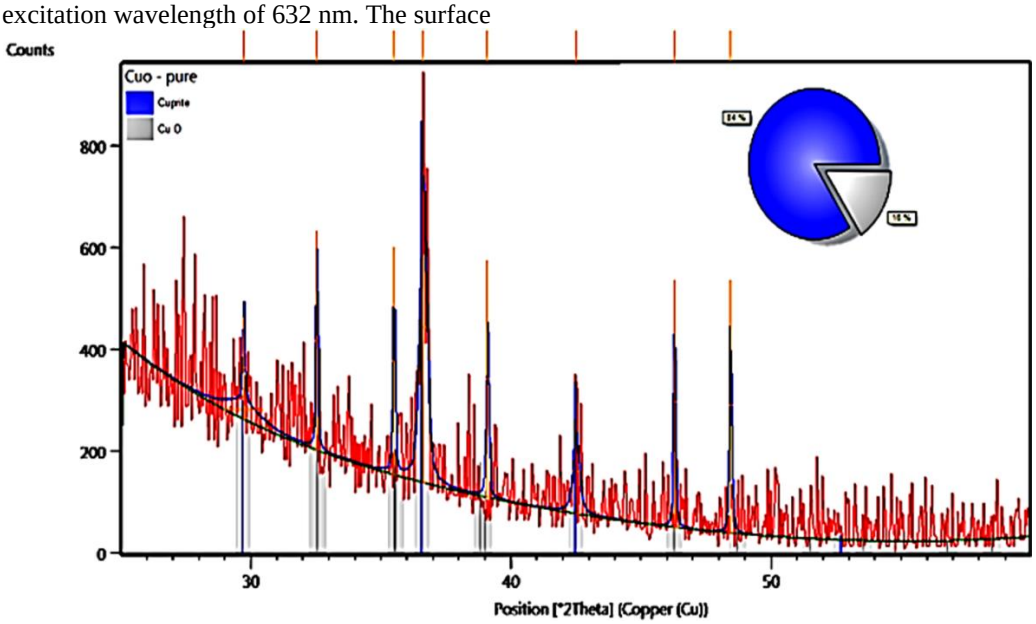

Fig. 1. Adjustment, using High Score Plus software, of the diffractograms corresponding to thin layers of copper oxide pure (color online)

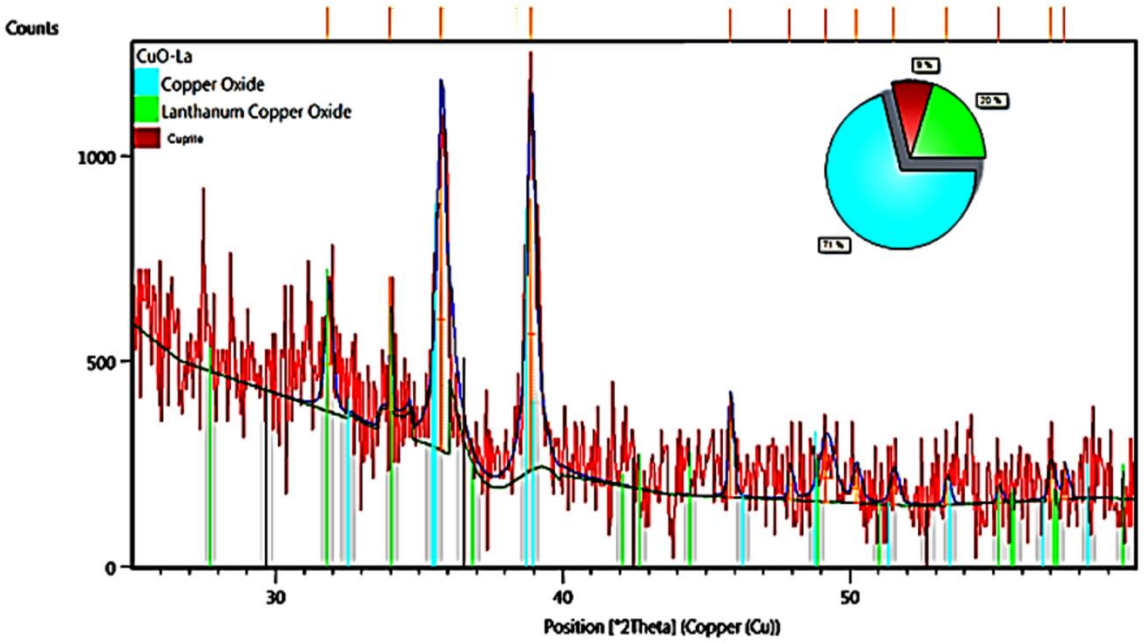

Fig. 2. Adjustment, using High Score Plus software, of the diffractograms corresponding to thin layers of copper oxide doped with 5% La (color online)

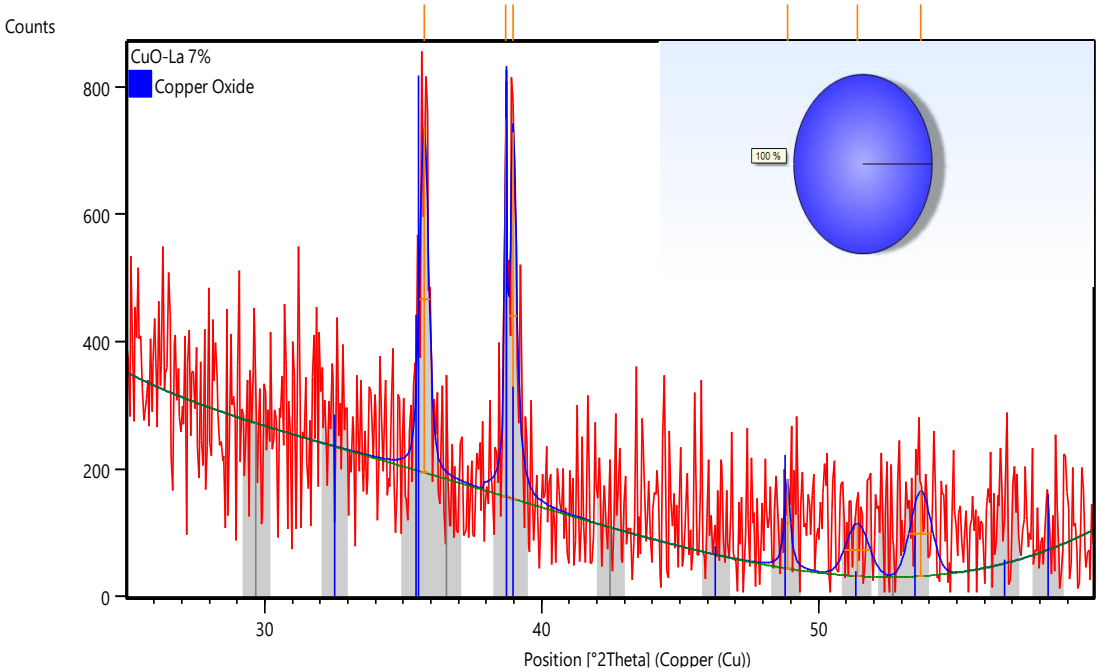

Fig. 3. Adjustment, using High Score Plus software, of the diffractograms corresponding to thin layers of copper oxide doped with 7% La (color online)

The structural parameters, such as grain size (D), FWHM (β), strain (ε), lattice spacing (d), and dislocation density (δ) for undoped and CuO: La nanocomposite thin films were estimated from the XRD patterns. The average value of the grains size was estimated from the XRD peaks, according to Debye Scherrer's formula [23]:

$$D = \frac{0{,}9\lambda}{\beta \cos\theta} \quad (1)$$

where D is the crystallite size, λ = 1.5418 Å is the X-ray wavelength, β the FWHM of the peak, and θ is Bragg's angle. The strain values were calculated from the following relation:

$$\varepsilon = \frac{\beta}{4\tan(\theta)} \quad (2)$$

The lattice spacing (d) values for all films were calculated using Bragg's equation:

$$2d \sin\theta = n\lambda \quad (3)$$

where n is the order of diffraction, λ is the wavelength of the X-ray pattern, and θ is the angle of X-ray diffraction. The dislocation density (δ), which indicates the density of defects in the CuO films, was calculated using the following equation:

$$\delta = \frac{1}{D^2} \quad (4)$$

where D is the crystallite size.

The lattices parameters were calculated using the following equations for CuO monoclinic structure and for CuO cubic structure respectively:

$$\frac{1}{d^2} = \frac{1}{(\sin\beta)^2}\left[\frac{h^2}{a^2} + \frac{k^2(\sin\beta)^2}{b^2} + \frac{l^2}{c^2} - \frac{2hl\cos\beta}{ac}\right] \quad (5)$$

$$\frac{1}{d_{hkl}^2} = \frac{h^2+k^2+l^2}{a^2} \quad (6)$$

where, d is the inter-planer distance and (h, k, and l) are Miller indices for the particular Bragg reflection.

Table 1. Structural parameters of CuO pure and CuO:La nanocomposites thin films

Echantillon	2θ(°)	(hkl)	FWHM(°)	D (nm)	d_{hkl} (Å)	δx10^{-4} (nm^{-2})	ε x10^{-3} (line^{-2}.m^{-4})	a (Å)	b (Å)	c (Å)
CuO pure	36.7	(111)	0.41508	21.00	2.1267	22.67	321.98	4.254	/	/
	42.6	(200)	0.44529	20.00	2.4508	25.00	300.58	4.255	/	/
CuO/La5%	35.8	($\bar{1}$11)	0.52109	16.75	2.5062	35.64	417.24	4.692	3.450	5.180
	35.8	(002)	0.52109	16.75	2.5062	35.64	417.24			
	38.9	(200)	0.44323	19.87	2.3135	25.32	324.87			
CuO/La7%	35.8	(002)	0.50322	17.34	2.5062	33.26	403.49	4.692	3.450	5.180
	35.8	($\bar{1}$11)	0.50322	17.34	2.5062	33.26	403.49			
	38.9	(200)	0.54036	19.87	2.3135	25.33	396.59			

Tables 1 calculate and tabulate the different parameters. As the dopant concentration is increased, it can be observed that the FWHM increases and the peak intensity increases too. This indicates that the strain factor caused by the synthesis method and the dopant used have reduced the crystallite size, increasing the dislocation density. It also confirms that the La^{3+} ions have replaced the Cu^{2+} lattice sites or interstitial sites in the sample, causing strain to be applied to the system.

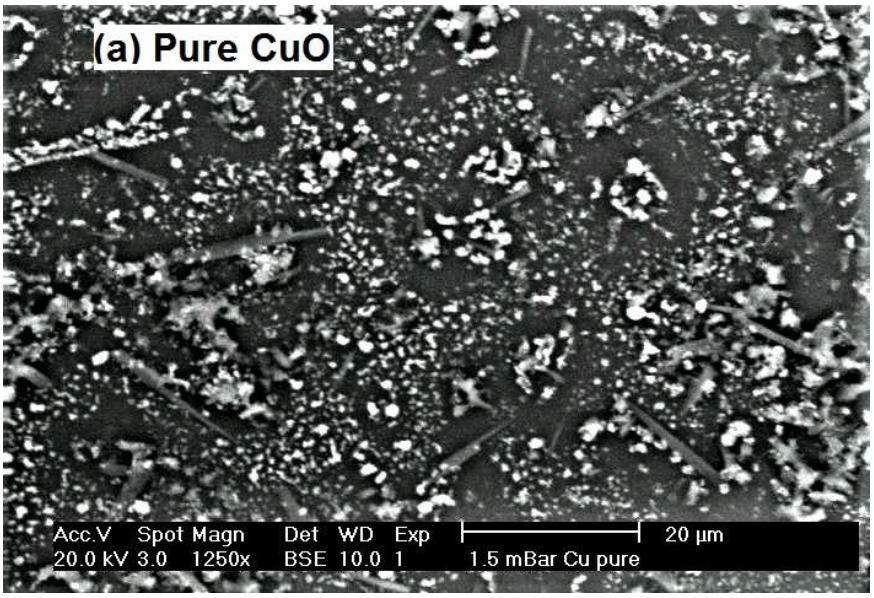

(a)

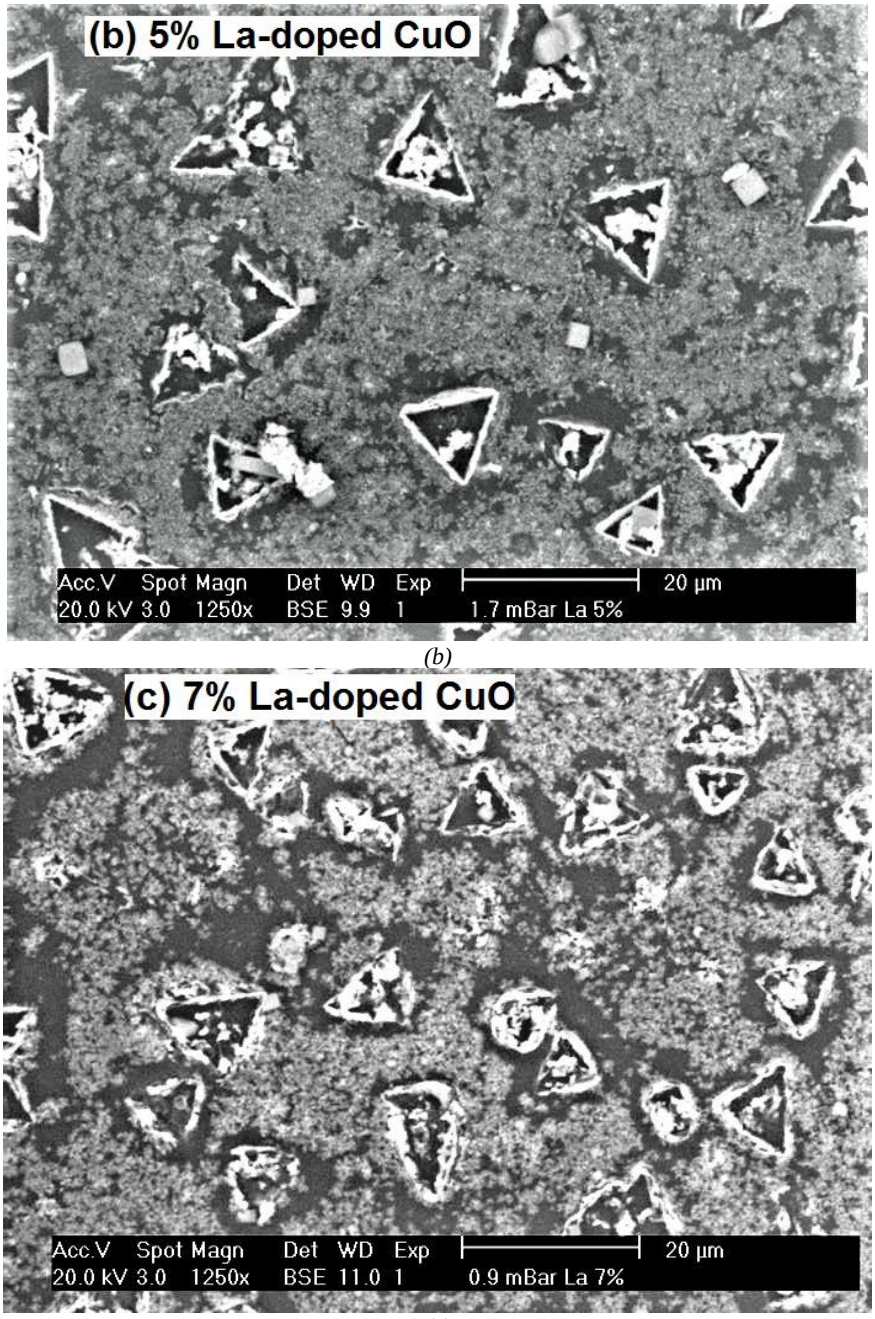

Fig. 4. SEM images of (a) undopped CuO thin film, (b) CuO:La 5% and (c) CuO:La 7%

The surface morphology of the prepared copper oxide thin films was revealed through the SEM image shown in Fig. 4 It shows a homogeneous particle distribution of the CuO/Cu_2O nanoparticles. By comparing the three micrographs, we see that the surface morphology of the doped samples presents a uniform and relatively dense surface with small pyramids enveloping the nanometric-sized crystallites. The pure sample surface morphology shows a homogeneous distribution of grains. It is also clear that the sizes of the crystallites are very small and difficult to see, which confirms the results found by XRD.

3.2. Raman analysis

Raman scattering spectra of CuO-Cu_2O copper oxide thin films were measured, as shown in Fig. 5. According to subsequent studies, the five peaks at 201, 300, 406, 489 and 638 cm^{-1} and the three peaks at 274, 328 and 627 cm^{-1} are the Raman fingerprints of Cu_2O and CuO, respectively [24]. The spectrum reveals the presence of two very distinct peaks at 285 and 335 cm^{-1} attributed to the A_g and $B_g(1)$ modes of copper oxide tenorite phase (CuO) respectively, and also notes the shift of these peaks towards high wavelengths (red shift). This shift is due to the quantum confinement induced by the small size of the crystallites.

The Raman spectra also reveal a shoulder spanning from 523 to 650 cm^{-1} attributed to the cuprite (Cu_2O) phase [25].

μ-Raman and XRD confirm the formation of two-phase copper oxide tenorite (CuO) and cuprite (Cu_2O) in all samples.

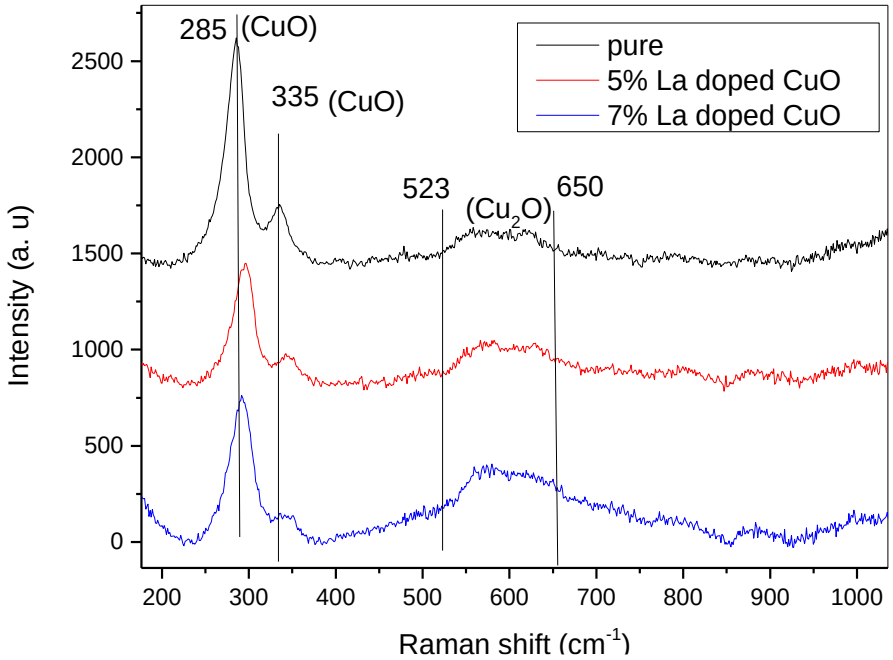

Fig. 5. Raman spectra of undoped CuO and CuO.La nanocomposites (color online)

3.3. Optical analysis

The optical properties of undoped CuO and La doped CuO thin films on glass substrates have been determined by using visible absorbance spectrum in the region of (250-900) nm, also calculate the optical energy gap for direct transition. The optical absorbance dependence on the wavelength (λ) in the spectra range 250-900 nm for undoped and doped CuO: La nanocomposites thin films measured at thicknesses of three layers are shown in Fig. 6. Films are higher absorption on the shorter wavelength side (ultraviolet region), and low absorption on the higher wavelength side (visible region). The spectra reveal that the absorbance was decreased by the increase in doping. The values of optical energy gap E_g for three samples have been determined using second differentiate are shown in Fig. 7. It found that the values of the gap are increasing with increasing concentration of La for all samples, and it found that the values increase from 1.3 to 1.43 eV.

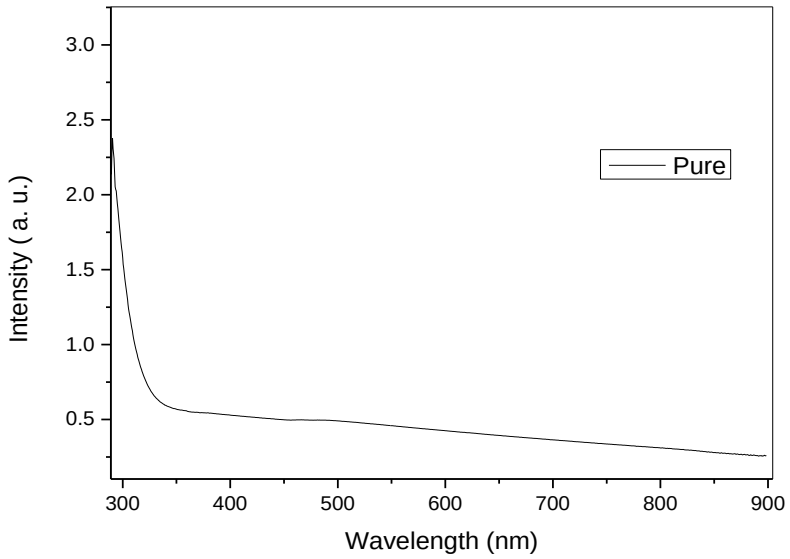

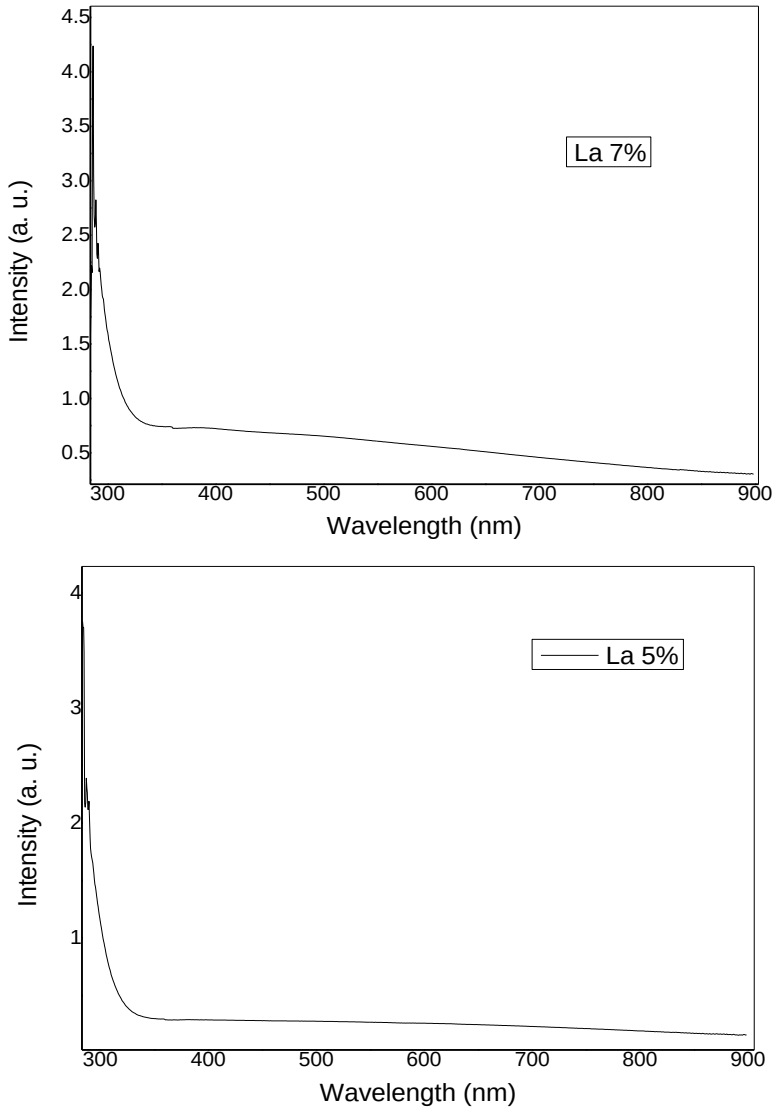

Fig. 6. Optical absorption spectra for undoped CuO and CuO:La nanocomposite thin films

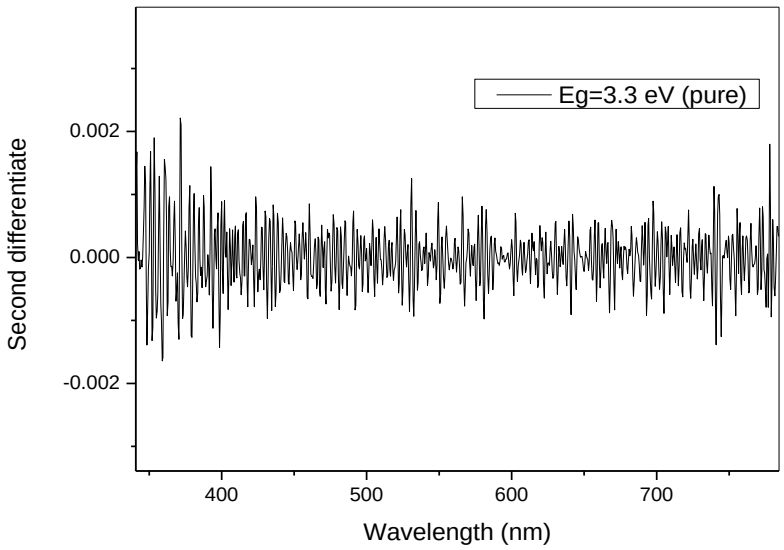

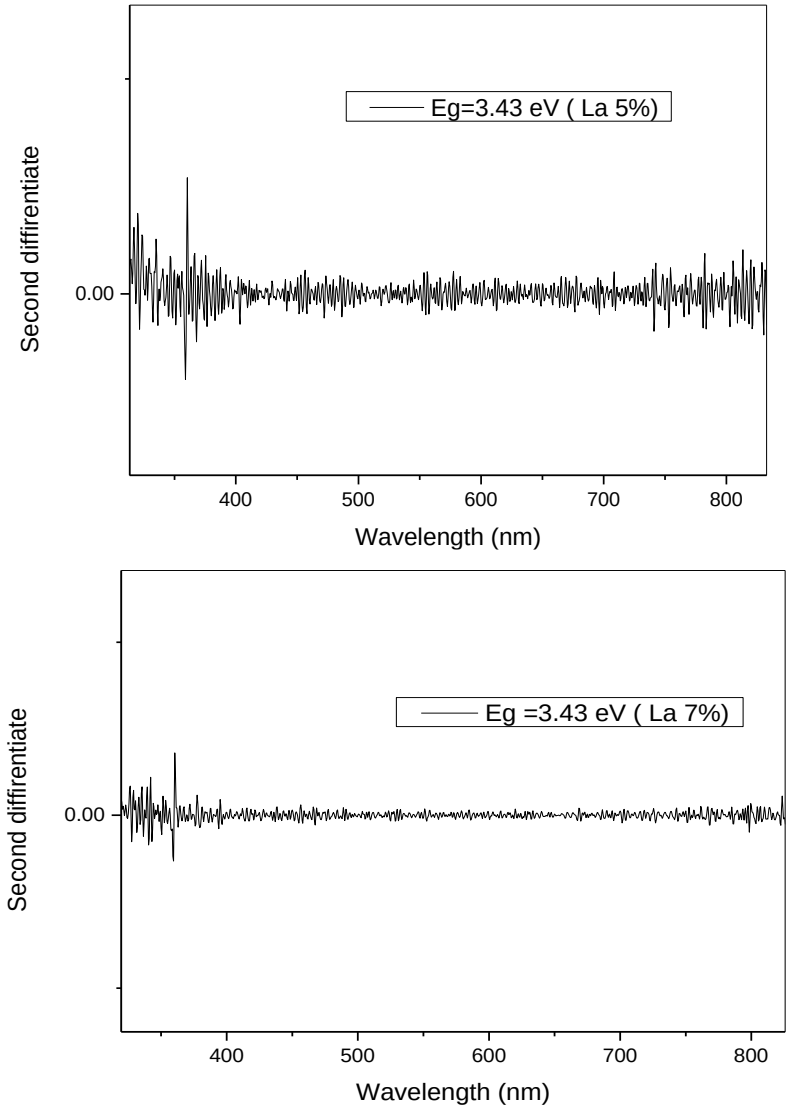

Fig. 7. Band gap energy for undoped CuO and CuO:La nanocomposite thin films

4. Conclusion

The physical properties of undoped CuO and La doped CuO nanocomposite thin films, deposited on glass substrates by a sol-gel method, were investigated. Structural analysis revealed the polycrystalline nature of the CuO and CuO: La nanocomposite thin films with a monoclinic and cubic structures, the crystallite size decreased. The SEM images of the CuO thin films showed that the La doping concentration affects the surface morphology of the CuO: La nanocomposite thin films. The spectra of the absorbance reveal that the absorbance was decreased by the increase in doping. The values of direct optical energy gap increasing with increasing concentration of La for all samples. The direct Eg increase from 1.3 to 1.43 eV, this blue shift is due to the quantum confinement induced by the reduction in the size of the crystallites.

References

[1] N. Y. Mostafa, A. Badawi, S. I. Ahmed, Results in Physics **10**, 126 (2018).
[2] M. Ponnar, C. Thangamani, P. Monisha, S. S. Gomathi, K. Pushpanathan, Applied Surface Science **449**, 132 (2018).
[3] M, Srivastava, J. Singh, R. K. Mishra, A. K. Ojha, Journal of Alloys and Compounds **555**, 123 (2013).
[4] A. Shuin, W. Zhu, L. Xu, D. Qin, Y. Wang, Ceramics International **39**, 8715 (2013).
[5] J. D. Rodney, S. Deepapriya, P. Annie Vinosha, S. Krishnan, S. Janet Priscilla, R. Daniel, S. Jerome Das, Optik **161**, 204 (2018).
[6] J. Morales, L. Sánchez, F. Martín, J. R. Ramos-Barrado, M. Sánchez, Thin Solid Films **474**(1), 133 (2005).
[7] S. P. Selvaraj, Materials Today Proceedings **50**, 7 (2020).

[8] A. Moumen, B. Hartiti, E. Comini, Z. El khalidi, H. M. M. M. Arachchige, S. Fadili, P. Thevenin, Superlattices and Microstructures **127**, 2 (2019).
[9] N. Anu, K. K. Thakur, K. K. Sharma, Inorganic and Nano-Metal Chemistry **50**(10), 933 (2020).
[10] A. A. Al-Ghamdi, M. H. Khedr, M. Shahnawaze Ansari, P. M. Z. Hasan, M. S. Abdel-Wahab, A. A. Farghali, Physica E: Low Dimensional Systems and Nanostructures **81**, 83 (2016).
[11] J. Zhao, Q. Liu, Y. Liu, Applied Surface Science **435**, 1212 (2018).
[12] A. Moumen, B. Hartiti, E. Comini, Z. El khalidi, H. M. M. M. Arachchige, S. Fadili, P. Thevenin, Superlattices and Microstructures **127**, 2 (2019).
[13] S. Ruzgar, Y. Caglar, O. Polat, D. Sobola, M. Caglar, Surfaces and Interfaces **21**, 100750 (2020).
[14] M. Srivastava, J. Singh, R. K. Mishra, A. K. Ojha, Journal of Alloys and Compounds **555**, 123 (2013)
[15] A. Shuin, W. Zhu, L. Xu, D. Qin, Y. Wang, Ceramics International **39**, 8715 (2013).
[16] J. Resende, O. Chaix-Pluchery, M. Rovezzi, Y. Malier, H. Renevier, N. D. Nguyen, J. L. Deschanvres, C. Jiménez, Journal of Physical Chemistry C **123**, 8663 (2019).
[17] Y. F. Lim, C. S. Chua, J. J. Lee, D. Chi, Physical Chemistry Chemical Physics **16**, 25928 (2014).
[18] K. Kardarian, P. M. Sberna, A. Ginsburg, D. A. Keller, J. V. Pinto, J. Deuermeier, A. Y. Anderson, A. Zaban, R. Martins, E. Fortunato Solar Energy Materials and Solar Cells **147**, 27 (2016).
[19] V. Ramya, K. Neyvasagam, R. Chandramohan, S. Valanarasu, A. M. F. Benial, Journal of Materials Science : Materials in Electronics **26**, 8489 (2015).
[20] F. Luo, J. Wei, Q. Liu, J. Wang, Materials Science in Semiconductor Processing **133**, 105972 (2021).
[21] K. P. Ganesan, N. Anandhan, G. Gopu, A. Amaliroselin, T. Marimuthu, R. Paneerselvam, Journal of Materials Science: Materials in Electronics **30**, 19524 (2019).
[22] N. Touka, D. Tabli, K. Badari, J. Optoelectron. Adv. M. **21**(11-12), 698 (2019).
[23] A. L. Patterson, Physical Review **56**, 978 (1939).
[24] L. C. Chen, C. C. Chen, K. C. Liang, S. H. Chang, Z. L. Tseng, S. C. Yeh, C. T. Chen, W. T. Wu, C. G. Wu, Nanoscale Research Letters **11**(1), 402 (2016).
[25] J. F. Xu, W. Ji, Z. X. Shen, W. S. Li, S. H. Tang, X. R. Ye, D. Z. Jia, X. Q. Xin, Journal of Raman Spectroscopy **30**, 413 (1999).

*Corresponding author: n.touka@univ-bouira.dz